Hindawi
International Journal of Antennas and Propagation
Volume 2020, Article ID 9128921, 11 pages
https://doi.org/10.1155/2020/9128921

Research Article

Parametric Analysis of Negative and Positive Refractive Index Lens Antenna by ANSYS HFSS

Phan Van Hung,[1] Nguyen Quoc Dinh,[1] Yoshihide Yamada,[2] Naobumi Michishita,[3] and Mohammad Tariqul Islam[4]

[1]*Faculty of Radio-Electronic Engineering, Le Quy Don Technical University, Hanoi, Vietnam*
[2]*Malaysia-Japan International Institute of Technology UTM, Kuala Lumpur, Malaysia*
[3]*National Defense Academy, Yokosuka, Kanagawa, Japan*
[4]*Department of Electrical, Electronic and Systems Engineering, Faculty of Engineering & Built Environment, Universiti Kebangsaan Malaysia, Bangi, Malaysia*

Correspondence should be addressed to Nguyen Quoc Dinh; dinhnq@mta.edu.vn

Received 2 June 2020; Revised 5 November 2020; Accepted 10 November 2020; Published 25 November 2020

Academic Editor: Ananda S. Mohan

Lens antennas with multibeam, high gain, and low sidelobe level are potential candidates for base station antennas in 5G mobile communication. In this paper, the authors perform simulation and parametric analysis of a lens antenna with positive and negative refractive indexes (NRI) using the modern electromagnetic field simulation software ANSYS HFSS. The simulation results of structures and theoretical calculations are analyzed and compared. The simulation results show the effectiveness of using negative refractive index lens antennas to minimize the dimension. The lens thickness with a negative refractive index decreased from 24.5 mm to 6.1 mm compared to the positive refractive index lens's thickness. The results also indicate the similarities in gain, sidelobe level, amplitude, and electric field distribution on the aperture plane of the negative and positive refractive indexes (PRI) lens antennas compared to the theoretical calculation. In addition, the authors simulate a lens structure with additional quarter wavelength matching layers (MLs) to estimate the antireflection performance.

1. Introduction

The fifth generation mobile system is now under development in the world [1–3]. The features of 5G in radio wave technology are millimeter wave frequency, small-size cells, and multiple input and multiple output (MIMO) systems [4, 5]. The new technology will allow a 5G antenna to low latency, low path loss, multibeam, beam scanning ability, broadband, and stable radiation pattern. In the massive MIMO, the base station antenna should assign one access line corresponding to one radio beam to one user [5, 6]. Thus, the base station antenna requires a multibeam radiation pattern like Figure 1. By using millimeter wave, the size of the base station antenna is reduced to about 30 cm; hence, types of antennas such as reflector, phased arrays, and dielectric lens antennas are proposed. As for a reflector antenna, a bifocal dual reflector and a reflectarray are proposed for multibeam application [7–9]. A phased array antenna is combined with a metasurface lens for extending the angular scan range, broadband, and multibeam [10–17]. As for a dielectric lens antenna, it has better multibeam radiation patterns than those of a dual reflector antenna, and this type of antenna also has structural features such as no blockage and having the same size beam forming surfaces of the front and rear surfaces, and stable radiation pattern [18–22]. However, on the downside, the thickness of dielectric lens antenna becomes larger. Meanwhile, when the refractive index is changed from the plus value to the minus value, the lens thickness can be remarkably reduced [23, 24]. In the study [25], the authors have designed simulated

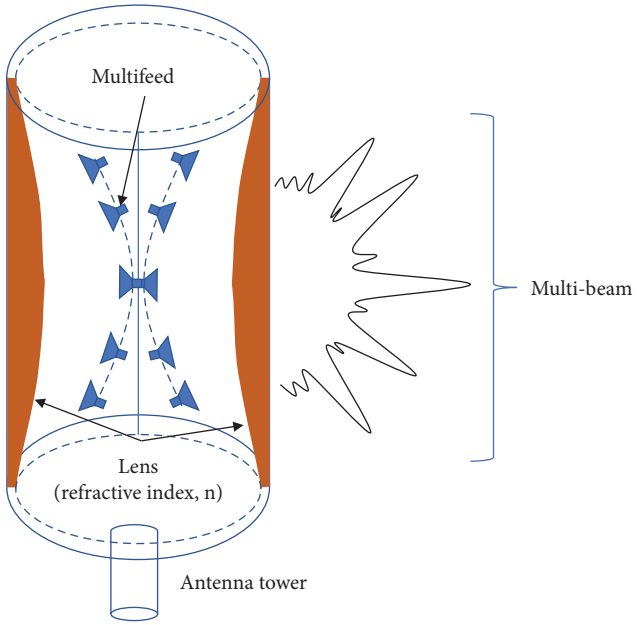

Figure 1: A multibeam lens antenna model for the base station.

electromagnetic fields and measured the structure of shaped dielectric lens antennas with refractive index $n = \sqrt{1.96}$ (Teflon) operating at 60 GHz using FEKO software. The results demonstrate very good agreements between the simulation results and the measured results.

However, there have been no studies of the simulation and comparison of negative and positive refractive index lens antennas in the electromagnetic environment. Therefore, in this paper, the authors research and simulate negative and positive refractive index lens antennas using ANSYS HFSS electromagnetic simulator. The value of the positive refractive index ($n = \sqrt{2}$) is approximately equal to that of Teflon refractive index ($n = \sqrt{1.96}$), which is studied and experimented in reference [25]. The comparison and analysis of lens size, gain, sidelobe level, and electric field distribution on the antenna planes and the effects of multiple reflections are performed. Also, the results are compared with the theoretical calculation of lens antennas. This paper consists of 5 sections. Section 2 shows the structures of lens antennas with negative and positive refractive indexes and fundamental expressions in determining the curve surface and the theoretical calculation of the lens antennas. Simulation conditions, parameters, and the matching layers structure are presented in section 3. Section 4 illustrates the simulation results, the comparison, and the discussion. Finally, the conclusions are summarized in section 5.

2. Antenna Structures

2.1. Lens Antenna Features and Structures. The geometries of the negative and positive refractive index lens antennas are shown in Figure 2. The lenses are rotationally symmetric around the Z-axis. The conical horn antenna is used as a feed. The lens materials have the refractive indexes of $n = -\sqrt{2}$ and $n = \sqrt{2}$. The lens has a basic structure, and its inner surface is curved and the outer surface is planar. The inner surface is generated by [20, 26, 27]

$$r = \frac{(n-1)F}{n\cos\theta - 1}, \tag{1}$$

where r is the distance from the focal point to the curve lens surface. The focal point is located at the origin of the coordinates axis. F is the distance between the focal point and the lens vertex. θ is the angle from the focal point to the inner lens surface and the Z-axis. n is a refractive index. ε_r is relative permittivity. μ_r is relative permeability. θ_i and θ_r indicate an incident angle and a refracted angle at a curve lens surface, respectively. These angles satisfy Snell's law.

$$n = \frac{\sin\theta_i}{\sin\theta_r}, \tag{2}$$

$$n = \sqrt{\varepsilon_r}\sqrt{\mu_r}. \tag{3}$$

The distance from the origin to the lens vertex and the diameter of the lens are $F = D = 100$ mm. T indicates the lens thickness. The rays from the feed horn are refracted at the curve lens surface, which makes outgoing rays parallel to the Z-axis.

For a symmetrical axis lens with a feed horn at focal point, in Figure 2, $E_p^2(\theta)\mathrm{d}\theta$ is the power radiated per unit length by the feed horn between the angles θ and $\theta + \mathrm{d}\theta$. Then, if $E_d^2(x)$ is the power per unit length in the corresponding aperture interval between x and $x + \mathrm{d}x$, where x is the distance ($x = r\sin\theta$) from a point on the aperture plane to the oz axis, from equation (1), x distance is given by the following equation:

$$x = \frac{F(n-1)\sin\theta}{n\cos\theta - 1}, \tag{4}$$

$$\frac{\mathrm{d}x}{\mathrm{d}\theta} = \frac{(n-1)F(n-\cos\theta)}{(n\cos\theta - 1)^2}. \tag{5}$$

Reflection from the lens surface is neglected. For the hyperbolic surface, the relationship between the electric field distribution on the aperture plane and the electric field of the feed horn is given by [27]

$$\frac{E_d^2(x)}{E_p^2(\theta)} = \frac{\mathrm{d}\theta}{\mathrm{d}x}. \tag{6}$$

From equations (5) and (6), the electric field distribution on the aperture plane is determined by:

$$E_d^2(x) = \frac{\mathrm{d}\theta}{\mathrm{d}x}E_p^2(\theta) = \frac{(n\cos\theta - 1)^3 E_p^2(\theta)}{(n-1)^2 F^2(n-\cos\theta)}. \tag{7}$$

Applying equation (1) to determine the points on the upper curve lens surface on the xz plane with the negative and positive refractive indexes is shown in Table 1.

2.2. Conical Horn Antenna Structures. The structure, fundamental dimensions, and the electric field of the conical horn antenna are illustrated in Figure 3(a). The feed horn is

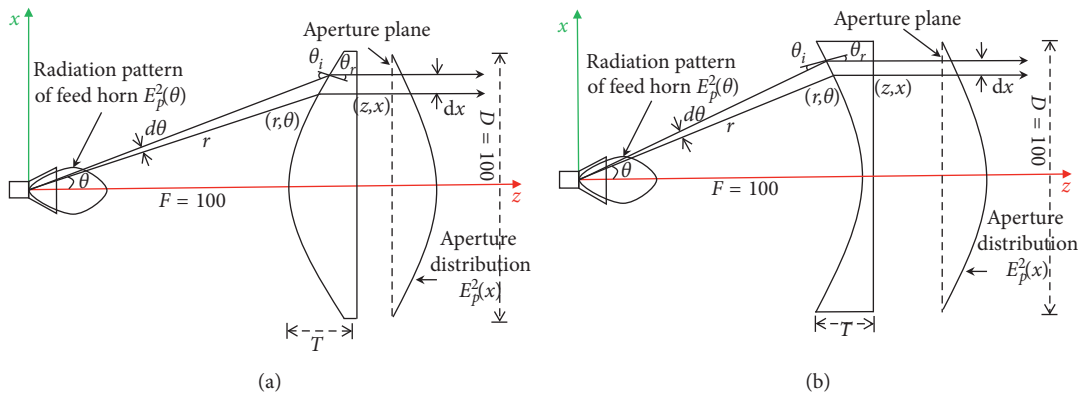

Figure 2: Lens antenna structures. (a) Horn with PRI lens ($n = \sqrt{2}$), (b) Horn with NRI lens ($n = -\sqrt{2}$).

Table 1: Points on curve lens surface ($F = D = 100$ mm).

θ	$n = \sqrt{2}$		$n = -\sqrt{2}$	
	x	z	x	z
0°	0	100	0	100
5°	8.83	100.9	8.7	99.8
10°	18.3	103.9	17.5	99.4
15°	29.3	109.3	26.4	98.6
20°	43.1	118.3	35.5	97.4
22.04°	50	123.5	39.2	96.8
25°			44.7	95.9
27.8°			50	94.9

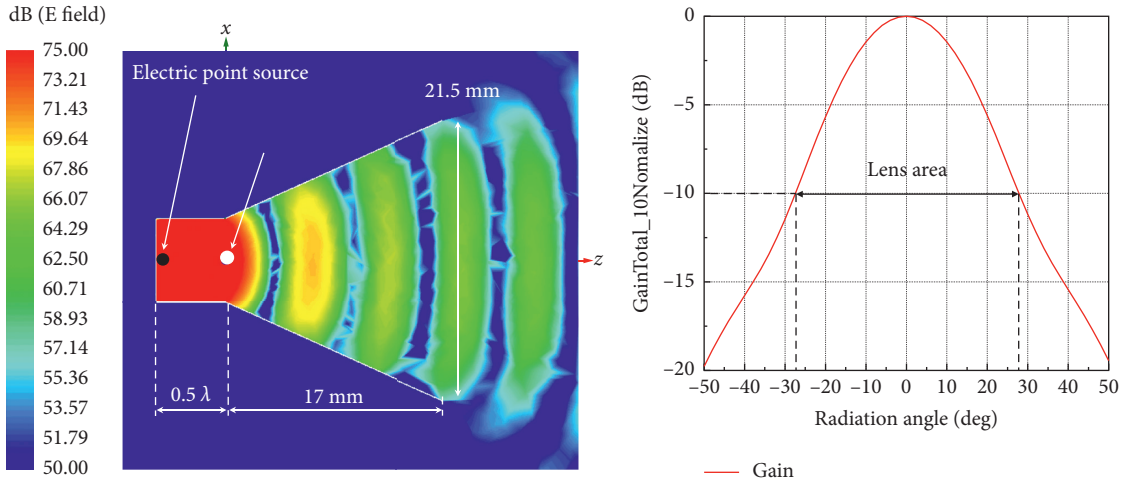

Figure 3: Parameters and the radiation pattern of the conical horn. (a) Conical horn antenna structure, (b) horn radiation patterns.

used to illuminate a wide angle for the lens. The radiation pattern of the conical horn antenna is shown in Figure 3(b). The horn has the maximum gain of 15.15 dBi. The lens area is stationed in the horn radiation angle (θ) from −27.8° to 27.8°, where the horn electromagnetic radiation obtains −10 dB compared to the maximum value. The focus of lens is set at center of the horn throat.

3. Designing Matching Layers and Simulation Conditions

3.1. Designing Matching Layers. A lens antenna with high-density dielectric material allows improving the energy transmission efficiency. However, using a lens whose material is a dielectric causes the worsening, which affects the

radiation properties of the antenna. These effects are due to multiple reflections on the curve surface and inside the lens. This can be overcome by covering the lens with matching layers. Matching layers thickness is limited to a quarter wavelength [28–32].

The designed lens structure with a quarter wavelength matching layers at the front and the rear of the lens and some layers parameters are shown in Figure 4, where ε_r is relative permittivity of the lens. ε_{ML} indicates permittivity of the matching layers ($\varepsilon_{ML} = \sqrt{\varepsilon_r}$). D_{ML} is the matching layer thickness ($D_{ML} = \lambda_g/4$). λ_g is the internal MLs wavelength.

3.2. Simulation Conditions and Parameters. The simulation parameters and the personal computer configurations are indicated in Table 2. The ANSYS HFSS and FEKO electromagnetic simulators are used to calculate the electrical field on the planes and the electric field distribution on the aperture plane based on designed structures. The Multilevel Fast Multipole Method (MLFMM) is applied simultaneously in order to optimize the calculation ability, save the computer memory, and minimize the calculation time. The lenses are set with the relative permeability $\mu_r = 1$ and $\mu_r = -1$ and the relative permittivity $\varepsilon_r = 2$ and $\varepsilon_r = -2$ corresponding to the refractive index of $n = \sqrt{2}$ and $n = -\sqrt{2}$, respectively. For the lenses with matching layers, the parameters are set: $\varepsilon_{ML} = \sqrt{2}$, $\varepsilon_{ML} = -\sqrt{2}$ and $D_{ML} \approx 2.25$. The distance between the focal point and lens vertex equals the diameter of the lens aperture ($F = D = 100$ mm). The survey frequency is 28 GHz.

4. Performance Results

4.1. The Electric Field Distribution on the yz Plane. Electric field distributions of a lens antenna with the refractive indexes of $n = \sqrt{2}$ and $n = -\sqrt{2}$ are shown in Figure 5. It is clearly observed that the radiation rays from the conical horn antenna are spherical waves, which are refracted and reformed when reaching the curve inner lens surface, and the waveforms at the outer surface are planar. This is correct in both cases of $n = \sqrt{2}$ and $n = -\sqrt{2}$, and this meets the theoretical conditions of the lens antennas. In order to ensure the simulation accuracy of HFSS software, a comparison with FEKO software is performed. In the study [25], the authors have made the design and simulation using FEKO and conducted experimental measurements of the shaped dielectric lens antenna structure with a positive refractive index ($n = \sqrt{1.96}$) operating on 60 GHz. The results in the study [25] show a similarity between simulation by FEKO and measured results. This demonstrates the simulation calculation accuracy of the FEKO software. Figure 5(c) shows the electromagnetic field distribution of a lens antenna with a positive refractive index ($n = \sqrt{2}$) when simulated by the FEKO software. Comparing the results between Figures 5(a) and 5(c), it can be seen that the antenna's field distribution with the positive refractive index is uniform when simulated by two different software tools, HFSS and FEKO. This proves the precision in constructing the structure and setting the methods and parameter calculations.

4.2. Radiation Patterns. The radiation patterns of the conical horn antenna and the lens antennas with different refractive indexes are illustrated in Figure 6. The green dashed dotted line shows the radiation pattern when $n = \sqrt{2}$, the blue dashed one represents the radiation pattern when $n = -\sqrt{2}$, and the black dashed squared line indicates the radiation pattern of conical horn antenna without lens. Clearly, the gain of the lens antenna when $n = -\sqrt{2}$ reaches 27.34 dBi while that of the lens antenna when $n = \sqrt{2}$ is 27.20 dBi, which are significantly higher than the gain of the conical horn antenna without lens, at 15.15 dBi. This demonstrates the effectiveness in improving the ability of the radiation properties of the lens antenna.

The red solid dotted line represents the PRI antenna's radiation pattern of the designed lens antenna with the same size, simulated by FEKO electromagnetic field software. The results show that the red solid dotted line and the green dashed dotted line are in good agreement. This shows the accuracy of the result in the simulation calculation using both software tools. Consequently, it can be concluded that the simulation results using HFSS software in the proposed model are accurate because the simulation process done by HFSS and FEKO software tools in the study [25] used the same calculation method, the multilevel fast multipole method (MLFMM). Thus, from the results of the electric field distribution, from Figures 5(a) and 5(c) and the radiation pattern of the lens antenna with a positive refractive index, we can see that the correlation results between the HFSS and FEKO software tools are done with the same calculation method to confirm the results' accuracy based on our proposed model.

The simulation results are indicated in Table 3. The sidelobe level in H-plane reaches the lowest value of -21.80 dB for a positive refractive index lens $n = \sqrt{2}$, and −20.17 dB for a negative refractive index lens $n = -\sqrt{2}$, while the sidelobe level of the conical horn antenna just gets −18.00 dB. Besides, the half power beam-widths (HPBW) of negative and positive refractive index lens antennas are fairly similar, at 7.78° and 7.13°, respectively. By contrast, the HPBW of a conical horn antenna without lens is 30.50°. The dimension of the lens is determined based on equation (1) and the structure-constructing method of using the simulator. From equation (1), we can see that when the refractive index of the lens is a positive value ($n = \sqrt{2}$), the inner curved surface structure of the lens is convex and directed towards the feed horn. The lens thickness at the center is a maximum, 24.5 mm. However, when the lens's refractive index has a negative value ($n = -\sqrt{2}$), the inner curved surface structure of the lens is concave, and the lens dimension has the thickest at the

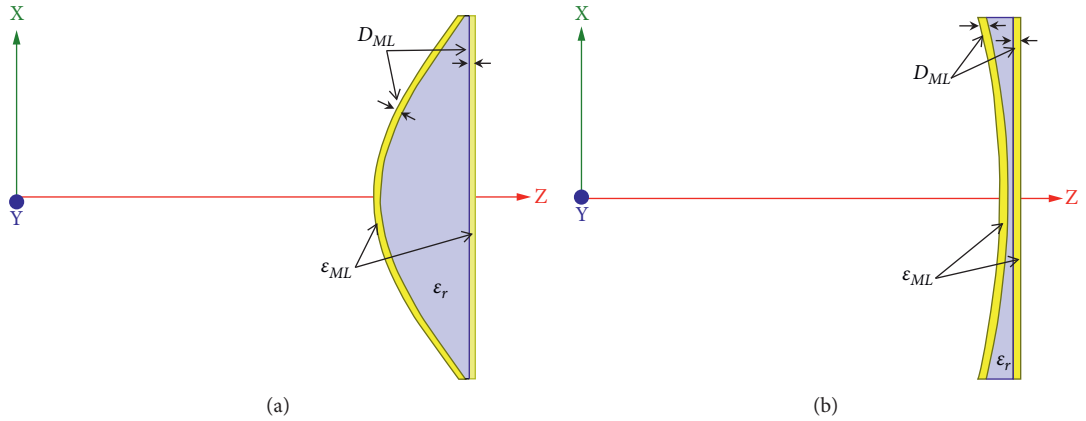

Figure 4: Lens structures with matching layers. (a) PRI lens with MLs. (b) NRI lens with MLs.

Table 2: Simulation parameters.

Computer specification	CPU		Intel xeon 5*E*	
	Loaded memory		128 GB	
	Software		HFSS and FEKO	
	Simulation method		MLFMM	
Positive and negative refractive index lens parameters	Lens diameter (mm)	D	100	
	Distance from the origin to the lens vertex (mm)	F	100	
	Relative permeability	μ_r	1	−1
	Relative permittivity	ε_r	2	−2
	Relative permeability MLs	ε_{ML}	$\sqrt{2}$	$-\sqrt{2}$
	Matching layer thickness (mm)	D_{ML}	2.25	
Survey frequency			28 GHz	

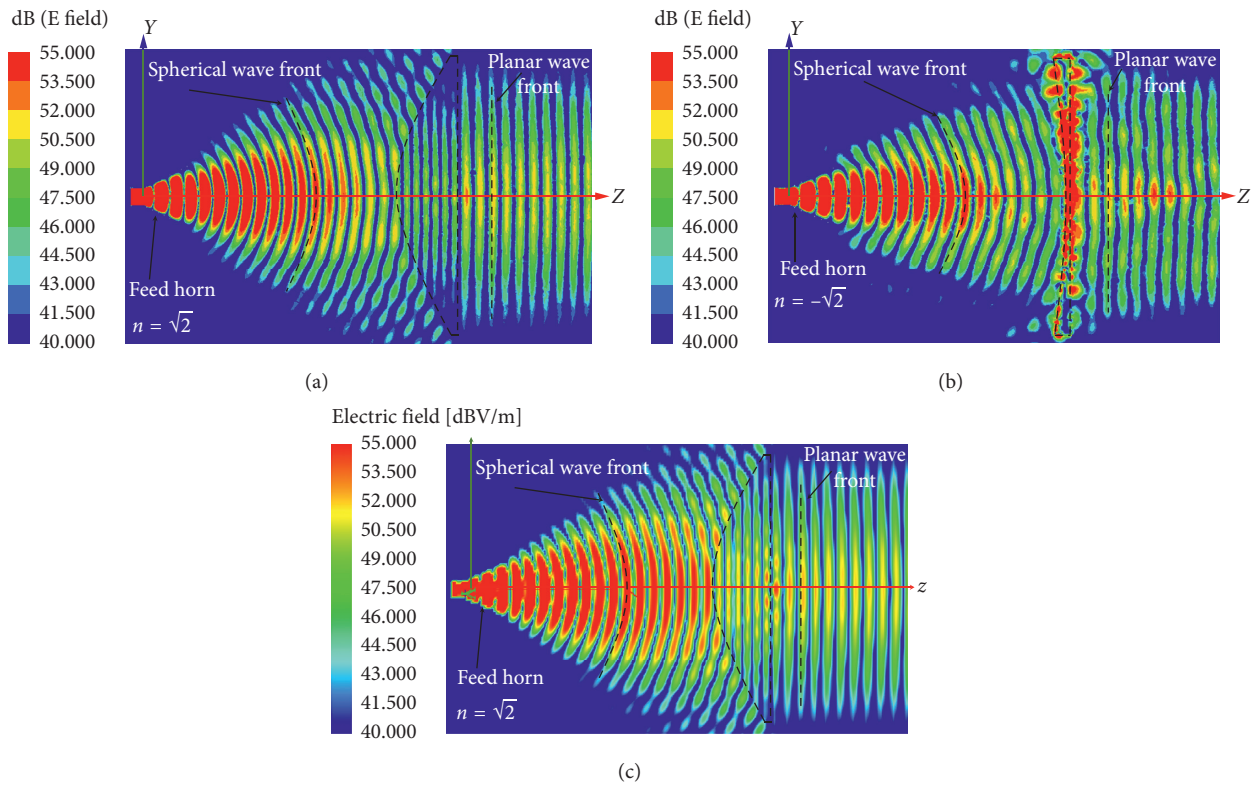

Figure 5: The electric field distributions on the yz plane. (a) PRI lens antenna ($n = \sqrt{2}$). (b) NRI lens antenna ($n = -\sqrt{2}$), (c) PRI lens antenna ($n = \sqrt{2}$) by FEKO.

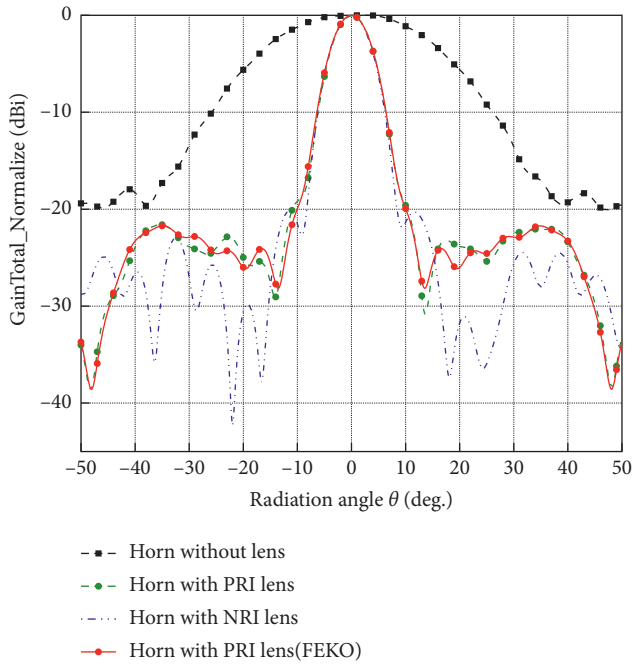

Figure 6: Radiation patterns of the horn antenna and the horn with PRI lens and NRI lens.

Table 3: Comparison results.

Antenna structures	n	Gain [dBi]	SLL (dB)	θ_B (deg.)	Lens thickness (mm)
Horn without lens		15.15	−18.00	30.50	
Horn with PRI lens	$\sqrt{2}$	27.20	−21.80	7.13	24.5
Horn with NRI lens	$-\sqrt{2}$	27.34	−20.17	7.78	6.1
Horn with PRI lens (FEKO)	$\sqrt{2}$	26.83	−21.73	7.23	24.5
PRI lens with MLs	$\sqrt[4]{2}$	27.80	−22.49	6.70	29.1
NRI lens with MLs	$-\sqrt[4]{2}$	27.30	−18.52	7.49	10.7

lens edge and is equal to 6.1 mm, which is significantly thinner than that of positive refractive index lens. As a result, negative refractive index lens antennas for base stations could be designed with smaller sizes reducing outer impacts.

4.3. The Electric Field Amplitude Distribution on the Aperture Plane. The electric field amplitude distributions on the aperture plane of the lens antennas for $n = \sqrt{2}$ and $n = -\sqrt{2}$ are shown in Figures 7 and 8. In Figure 7, it is obvious that electric field distributions in both cases are uniform and symmetric around the Z-axis. In addition, Figure 8 shows that the electric field amplitude distribution of the lens antenna is theoretically calculated according to equation (7) and simulated with positive and negative refraction indexes. Thus, electric field amplitudes on the aperture plane distributed along the lens diameter line are high and tend to decrease gradually to the sides. The simulation results and theoretical calculations are quite similar. This shows the accuracy in the design and theoretical calculations. The ripples on the amplitude distribution lines in case of the simulation occur due to the reflection from the lens surface.

4.4. The Effects of Matching Layers. The comparisons of the radiation patterns of the different refractive index lens antennas with and without matching layers on the yz plane are illustrated in Figure 9. It can be observed that when utilizing quarter wavelength matching layers for the positive refractive index lens, the antenna gain increases by 0.60 dBi compared to the one without quarter wavelength matching layers, whereas the antenna gain is almost unchanged when using MLs for negative refractive index lens. The sidelobe

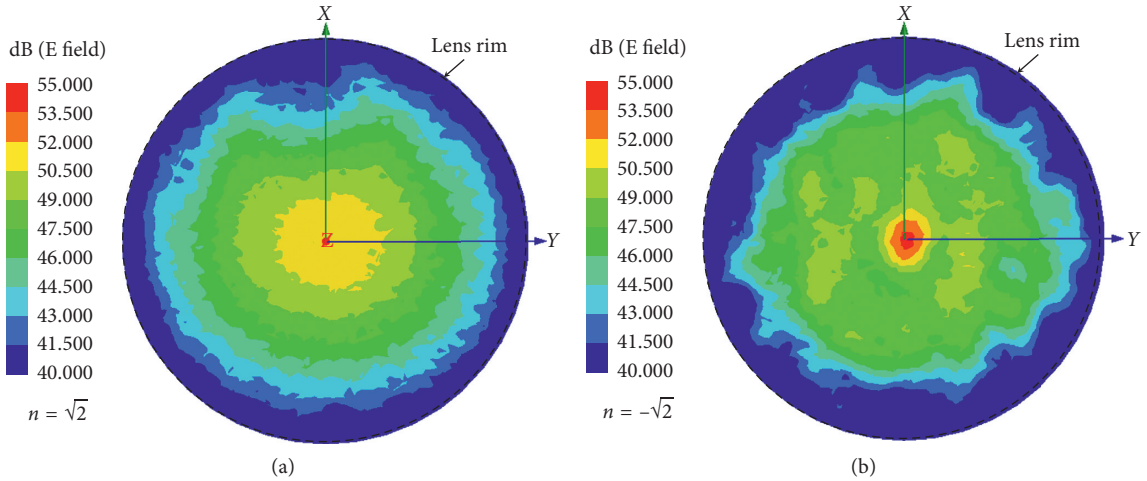

FIGURE 7: The electric field distributions on the aperture plane. (a) PRI lens ($n = \sqrt{2}$). (b) NRI lens ($n = -\sqrt{2}$).

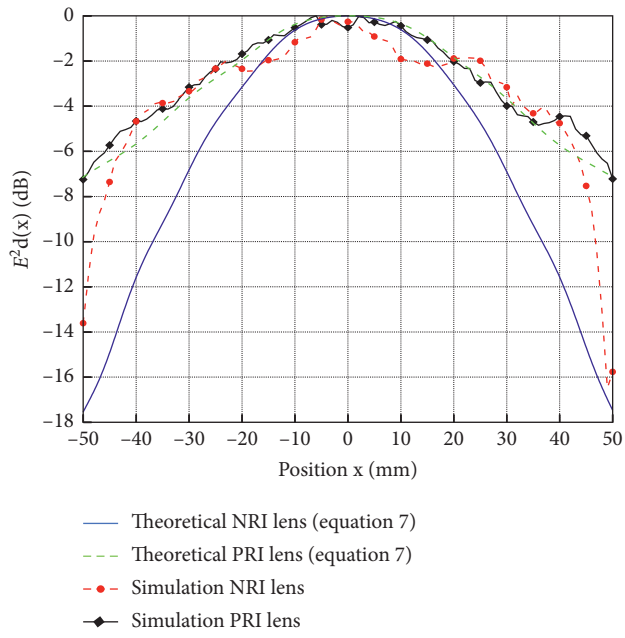

FIGURE 8: The comparison of electric field amplitude distributions on the aperture plane for PRI and NRI lens antennas based on theoretical and simulation.

level in H-plane also decreases from −21.80 dB to −22.49 dB with positive refractive index lens antennas and increases from −20.17 dB to −18.52 dB with negative refractive index lens antennas. The results show the efficiency of using a quarter wavelength matching layers for a positive refractive index lens antenna.

The investigation into the electric field distribution of lens antennas with and without quarter wavelength matching layers is presented in Figure 10. Spillover and diffraction occur more clearly at the lens edge for a positive refractive index. In Figure 11, the electric field amplitude distributions on the aperture planes between the antenna lens with and without the quarter wavelength matching layers are compared with each other. The results show that, in the case of the positive refractive index lens antennas, the black solid line, which illustrates the field amplitude distribution of the lens antenna with matching layers, is smoother and less jagged than the red dashed one presenting the case without matching layers. In contrast, the field amplitude distribution line of the negative refractive index

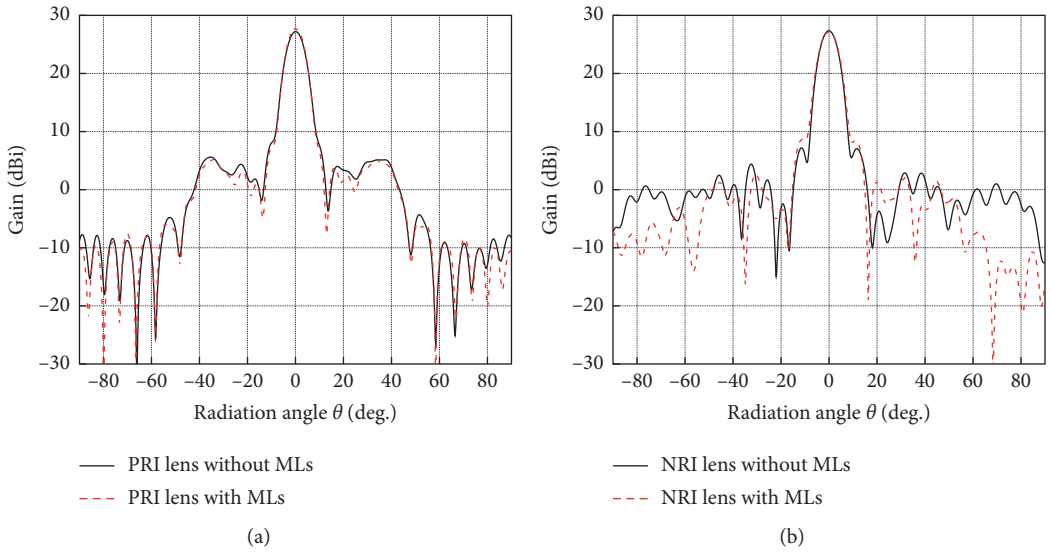

Figure 9: The comparison of radiation patterns of lens antennas on the yz plane. (a) PRI lens with and without MLs. (b) NRI lens with and without MLs.

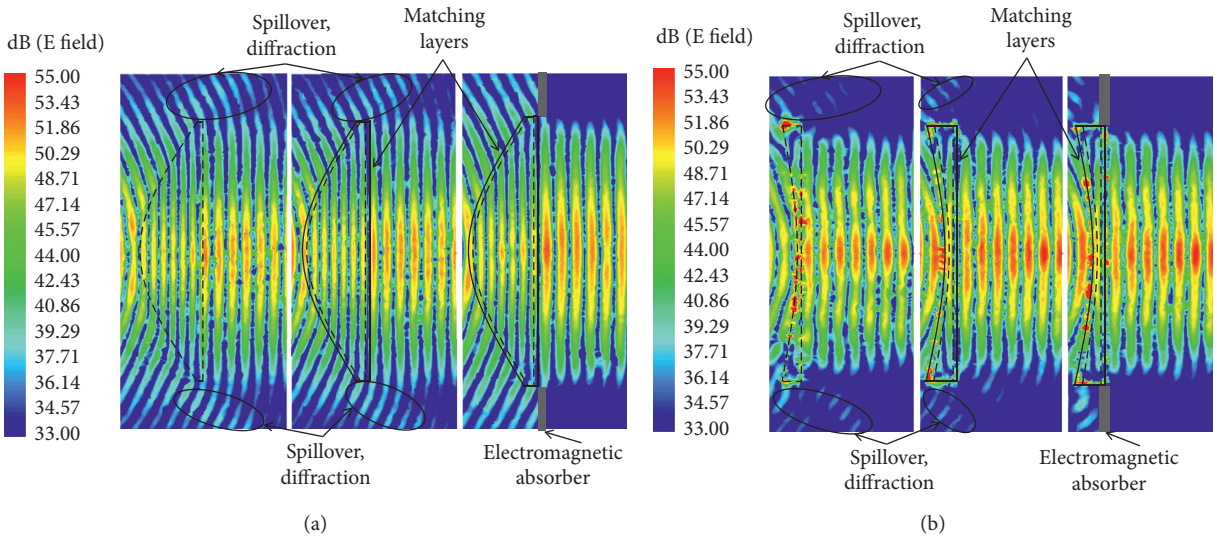

Figure 10: The electric field distributions of lens antennas with and without the quarter wavelength matching layers. (a) PRI lens. (b) NRI lens.

lens antenna with matching layers is even more rugged than without MLs. This shows the more uniform electric field distribution on the aperture plane of the positive refractive index lens antennas when using the quarter wavelength matching layers.

The authors use the ray tracing method to investigate the effects of multiple reflection from the curve lens surface, as shown in Figure 12. Accordingly, black solid lines are the incident rays that travel from the focal point to the inner surface of the lens where the refraction and reflection phenomena occur. Most of the parts of the incident ray power are refracted, which makes outgoing rays parallel to the Z-axis, the solid red lines, while the rest are reflected at the curve surface, the blue dashed lines. This phenomenon causes spillover and diffraction. As to the positive refractive index lens, the lens structure is convex. Thus, reflected rays from the curve lens surface tend towards diffraction at the lens edge. Meanwhile, reflected rays from negative refractive

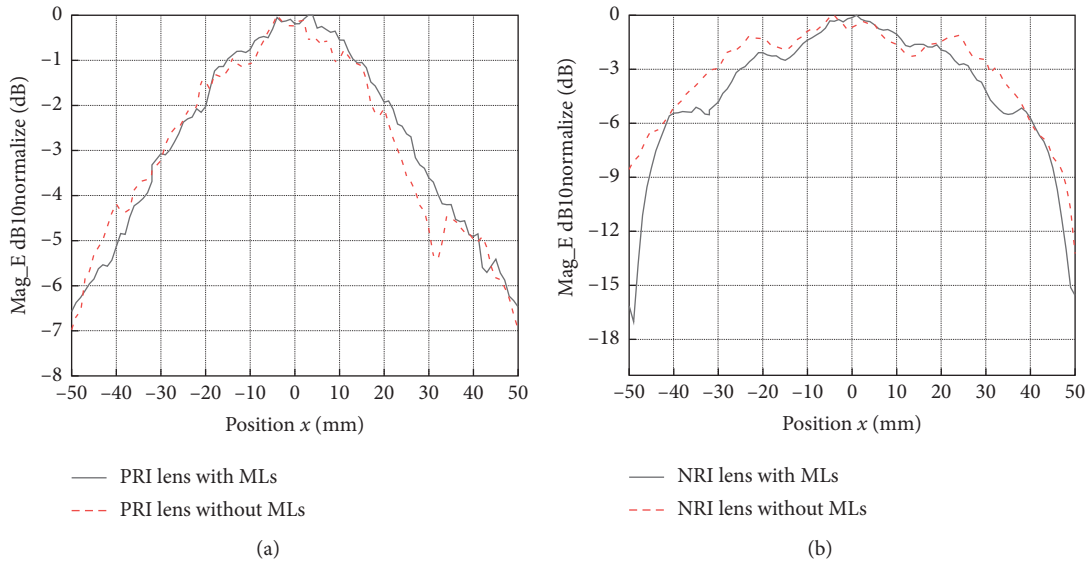

Figure 11: Electric field amplitude distributions on the aperture planes. (a) PRI lens with and without MLs. (b) NRI lens with and without MLs.

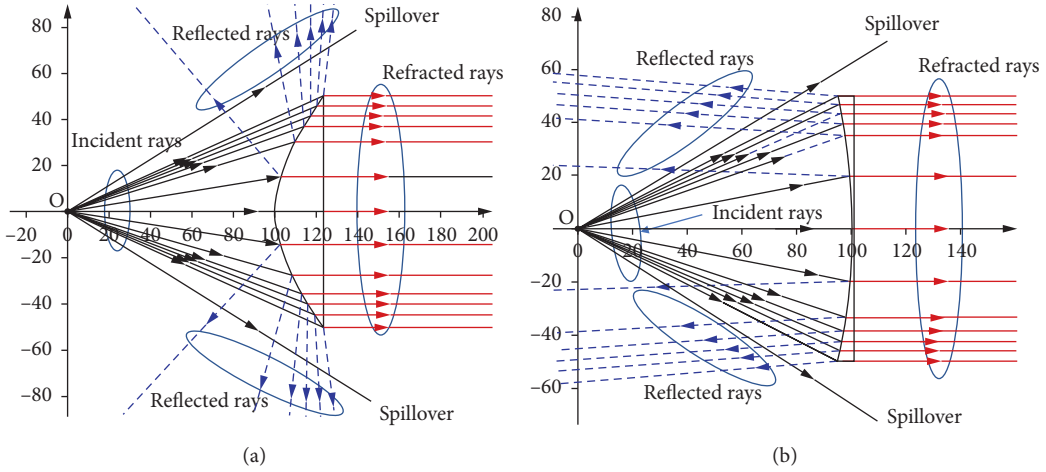

Figure 12: Multiple reflected rays on the curve lens antenna surface. (a) PRI lens. (b) NRI lens.

index lens surface tend to bounce back because of the concave lens structure. Spillover and diffraction can be solved by covering the lens with an electromagnetic absorber, shown as in the third picture of Figures 10(a) and 10(b).

5. Conclusions

Two types of antennas with the positive and negative refractive index lens are simulated by using the electromagnetic simulator ANSYS HFSS. The result accuracy is verified by comparing the obtained antenna parameters with the theoretical calculations. The findings show that when the negative refractive index material is used, the lens thickness is 6.1 mm, which is significantly smaller than that of the positive refractive index material, at 24.5 mm. Further, sidelobe levels are also maintained at a low level, as shown in Table 3. Those results show the effectiveness of using negative refractive index lens antennas in constructing base station antennas. In addition, when investigating the antenna structure, quarter wavelength matching layers are added to the lens to reduce reflection from the curve surface. The results show that the matching layers are an effective choice for improving the radiation properties of a positive refractive index lens antenna.

Data Availability

The data used to support the findings of this study are available from the corresponding author upon request.

Conflicts of Interest

The authors declare that there are no conflicts of interest regarding the publication of this paper.

Acknowledgments

This research was funded by Vietnam National Foundation for Science and Technology Development (NAFOSTED) under grant no. 102.04-2018.08.

References

[1] W. Hong, Z. H. Jiang, C. Yu et al., "Multibeam antenna technologies for 5G wireless communications," *IEEE Transactions on Antennas and Propagation*, vol. 65, no. 12, pp. 6231–6249, 2017.

[2] L. Guangyi and J. Dajie, "5G: vision and requirements for mobile communication system towards Year 2020," *Chinese Journal of Engineering*, vol. 2016, Article ID 5974586, 8 Pages, 2016.

[3] S. Kumar, A. S. Dixit, R. R. Malekar, H. D. Raut, and L. K. Shevada, "Fifth generation antennas: a comprehensive review of design and performance enhancement techniques," *IEEE Access*, vol. 8, pp. 163568–163593, 2020.

[4] S. Sun, T. Rappaport, R. Heath, A. Nix, and S. Rangan, "MIMO for millimeter-wave wireless communications: beamforming, spatial multiplexing, or both?" *IEEE Communications Magazine*, vol. 52, no. 12, pp. 110–121, 2014.

[5] N. Vukmirovic, M. Janjic, P. M. Djuric, M. Erić et al., "Position estimation with a millimeter-wave massive MIMO system based on distributed steerable phased antenna arrays," *EURASIP J ADV SIG PR*, vol. 2018, pp. 1–17, 2018.

[6] J. Zhang, E. Björnson, M. Matthaiou, D. W. K. Ng et al., "Prospective multiple antenna technologies for beyond 5G," *in IEEE Journal on Selected Areas in Communications*, vol. 38, pp. 1637–1660, 2019.

[7] A. N. Plastikov and B. L. Kogan, "Bifocal reflector antenna design procedure for wide-angle multi-beam applications," in *Proceeding of the European Conference on Antennas and Propagation (EuCAP)*, Gothenburg, Sweden, Apr 2013.

[8] K. Ueno, "Multibeam antenna using a phased array fed reflector," in *Proceeding of the IEEE Antennas and Propagation Society International Symposium 1997*, pp. 840–843, Orlando, FL, USA, August 1997.

[9] Y. Chen, H. Meng, Y. Gan, and W. Dou, "Millimeter wave multi-beam reflector antenna," in *Proceeding of the 2018 International Workshop on Antenna Technology (iWAT)*, pp. 1–3, Nanjing, China, March 2018.

[10] F. Fan, M. Cai, J. Zhang, Z. Yan, and J. Wu, "Wideband low-profile luneburg lens based on a glide-symmetric metasurface," *IEEE Access*, vol. 8, pp. 85698–85705, 2020.

[11] K. L. Chung, S. Chaimool, and C. Zhang, "Wideband sub-wavelength-profile circularly polarised array antenna using anisotropic metasurface," *Electronics Letters*, vol. 51, no. 18, pp. 1403–1405, 2015.

[12] G. A. Egorov and G. V. Eleftheriades, "Theory and simulation of metasurface lenses for extending the angular scan range of phased arrays," *IEEE Transactions on Antennas and Propagation*, vol. 68, no. 5, pp. 3705–3717, 2020.

[13] K. L. Chung, X. Yan, S. Chaimool, B. Feng, and Y. Li, "On the surface susceptibilities and effective parameters of metasurfaces composed of isolated metallic unit-cells," *International Journal of RF and Microwave Computer-Aided Engineering*, pp. 1–9, 2020.

[14] C. Xue, Q. Lou, and Z. N. Chen, "Broadband double-layered huygens' metasurface lens antenna for 5G millimeter-wave systems," *IEEE Transactions on Antennas and Propagation*, vol. 68, no. 3, pp. 1468–1476, 2020.

[15] O. Yesilyurt and G. Turhan-Sayan, "Metasurface lens for ultra-wideband planar antenna," *IEEE Transactions on Antennas and Propagation*, vol. 68, no. 2, pp. 719–726, 2020.

[16] Y.-H. Lv, X. Ding, B.-Z. Wang, and D. E. Anagnostou, "Scanning range expansion of planar phased arrays using metasurfaces," *IEEE Transactions on Antennas and Propagation*, vol. 68, no. 3, pp. 1402–1410, 2020.

[17] N. Q. Dinh, N. T. Binh, Y. Yamada, and N. Michishita, "Proof of the density tapering concept of an unequally spaced array by electric field distributions of electromagnetic simulations," *Journal of Electromagnetic Waves and Applications*, vol. 34, no. 5, pp. 668–681, 2020.

[18] F. Ansarudin, T. Abd Rahman, Y. Yamada, N. H. A. Rahman, and K. Kamardin, "Multi beam dielectric lens antenna for 5G base station," *Sensors*, vol. 20, no. 20, p. 5849, 2020.

[19] S. A. Hamid, N. H. A. Rahman, Y. Yamada, P. V. Hung, and D. N. Quoc, "Multibeam characteristics of a negative refractive index shaped lens," *Sensors*, vol. 20, no. 19, p. 5703, 2020.

[20] Y. Tajima and Y. Yamada, "Design of shaped dielectric lens antenna for wide angle beam steering," *Electronics and Communications in Japan (Part III: Fundamental Electronic Science)*, vol. 89, no. 2, pp. 1–12, 2006.

[21] H. Giddens and Y. Hao, "Multibeam graded dielectric lens antenna from multimaterial 3-D printing," *IEEE Transactions on Antennas and Propagation*, vol. 68, no. 9, pp. 6832–6837, 2020.

[22] T. Maruyama, K. Yamamori, and Y. Kuwahara, "Design of multibeam dielectric lens antennas by multiobjective optimization," *IEEE Transactions on Antennas and Propagation*, vol. 57, no. 1, pp. 57–63, 2009.

[23] P. V. Hung, N. Q. Dinh, Y. Yamada et al., "Electromagnetic simulation method of a negative refractive index lens antenna," in *Proceeding of 2019 International Conference on Advanced Technologies for Communications (ATC)*, pp. 109–112, Hanoi, Vietnam, October 2019.

[24] S. Hamid, M. T. Ali, Y. Yamada, N. H. Abd Rahman, and N. Michishita, "Application of negative index lens antenna for 5G mobile base station," in *Proceeding Of 2018 International Symposium On Antennas And Propagation (ISAP)*, pp. 1-2, Busan, South Korea, October 2018.

[25] Y. Tajima and Y. Yamada, "Simulation of a shaped dielectric lens antenna by FEKO," *Applied Computational Electromagnetics Society Journal*, vol. 24, no. 4, pp. 419–426, 2009.

[26] Y. T. Lo and S. W. Lee, *"Lens Antenna," in Antenna Handbook, Theory, Applications, and Design*, pp. 5–23, Van Nostrand Reinhold, New York, USA, 1988.

[27] S. Sliver, "Dielectric and metal-plate lens," in *Microwave Antenna Theory And Design*, pp. 388–395, McGraw-Hill, New York, USA, 1986.

[28] N. T. Nguyen, R. Sauleau, and C. J. M. Perez, "Very broadband extended hemispherical lenses: role of matching layers for bandwidth enlargement," *IEEE Transactions on Antennas and Propagation*, vol. 57, no. 7, pp. 1907–1913, 2009.

[29] F. Tokan, *Matching Layer Design Procedure for a Novel Broadband Dielectric Lens Antenna*, pp. 149–198, 2103.

[30] M. G. M. V. Silveirinha and C. A. Fernandes, "Shaped double-shell dielectric lenses for wireless millimeter wave

communications," in *Proceedings of the IEEE Antennas and Propagation Society International Symposium. Transmitting Waves of Progress to the Next Millennium 2000 Digest. Held in conjunction with: USNC/URSI National Radio Science Meeting (Cat. No.00CH37118)*, Salt Lake City, UT, USA, July 2000.

[31] E. M. T. Jones and S. B. Cohn, "Surface matching of dielectric lenses," *Journal of Applied Physics*, vol. 26, no. 4, pp. 452–457, 1955.

[32] T. Morita and S. B. Cohn, "Microwave lens matching by simulated quarter-wave transformers," *IRE Transactions on Antennas and Propagation*, vol. 4, no. 1, pp. 33–39, 1956.